IEEE Access
Multidisciplinary | Rapid Review | Open Access Journal

Received March 22, 2019, accepted March 31, 2019, date of publication April 4, 2019, date of current version April 18, 2019.

Digital Object Identifier 10.1109/ACCESS.2019.2909274

Deep-Discharging Li-Ion Battery State of Charge Estimation Using a Partial Adaptive Forgetting Factors Least Square Method

SHIQI LIU[1], JUNHUA WANG[1], (Member, IEEE), QISHENG LIU[1], JIA TANG[1], HAOLU LIU[1], AND ZHIJIAN FANG[2], (Member, IEEE)

[1]School of Electrical Engineering and Automation, Wuhan University, Wuhan 430072, China
[2]School of Automation, China University of Geosciences, Wuhan 430074, China

Corresponding author: Junhua Wang (junhuawang@whu.edu.cn)

This work was supported in part by the National Natural Science Foundation of China under Project 51707138 and Project 51507114, and in part by the National Key Research and Development Plan under Project 2017YFB1201003-21 and Project 2017YFB1201002.

ABSTRACT State of charge (SOC) estimation of deep-discharging Li-ion batteries under complicated working conditions at different temperatures is still challenging. Nowadays, the depth of discharge (DOD) of batteries in electric vehicles (EVs) is generally low, resulting in the insufficient use of battery energy. This paper proposes a SOC estimation method using a novel partial adaptive forgetting factors recursive least square (PAFFRLS), which adjusts the forgetting factors based on the own physical properties of each parameter in equivalent circuit models (ECMs) to accommodate to greatly changing under deep-discharging range and high dynamic working conditions. The gain matrix in the proposed method is split to update independently according to each parameter, which solves the issue of mutual influence between parameters vary with different rates. In addition, four typical test profiles, including DST, UDDS, US06, and EUDC, are employed to simulate different working conditions of EVs. Eventually, numerous simulations and experiments results at different temperatures are employed to verify the validity of the proposed method. All average errors of the SOC estimation under four different kinds of working conditions are less than 1.3% as well as all peak errors are less than 5%. All peak errors are less than 3% while DOD is larger than 90%, which illustrates the effectiveness of the proposed method in the case of deep-discharging and provides better guidance to the design of battery management system (BMS) in EVs.

INDEX TERMS Deep-discharging Li-ion battery, battery equivalent circuit analysis, state of charge estimation, partial adaptive forgetting factors, parameter identification.

I. INTRODUCTION

The implementation of electric vehicle (EVs) is important as the global warming, climate change and greenhouse gas emissions caused by diesel, petrol-based vehicles [1]. Lithium-ion batteries are now the leading candidate for commercial use due to their desirable merits such as high energy density, design flexibility, and long lifespan [2]. However, state of charge (SOC) estimation of deep-discharging Li-ion battery under complicated working conditions is still challenging in EVs. The depth of discharge (DOD) of batteries in EVs is generally less than 80% nowadays, resulting in the insufficient use of battery energy. Therefore, accurate SOC estimation for deep-discharging Li-ion batteries under complicated conditions is significant for improving the mileage range of EVs.

The battery SOC estimation methods can be classified into two groups, including model-free and model-based methods [3]. As for model-free methods, ampere-hour integral method is easy to implement but the initial value is difficult to determine during the whole working condition, and the error may accumulate if the current measurements are not accuracy [4]. As for looking-up table based method, batteries must be settled a long time to recovery which is not appropriate for online SOC estimation [5]. The data driven methods such as Neural Network [1], [6], Support Vector Regression (SVR) model [7], Metabolic Grey Model [8], and so on, are very sensitive to their parameters and they may not

The associate editor coordinating the review of this manuscript and approving it for publication was Xiaosong Hu.

even be convergent with bad parameters selection when the training data cannot completely cover the present operating conditions. On the contrary, model-based methods including electrochemical model and equivalent circuit model (ECM) are effective methods to estimate the state of the battery. The electrochemical model is precise but it depends much on the parameter which is quite hard to measure. Also it is hard to solve the complicated partial differential equations of the electrochemical model [9]. ECMs utilize a combination of battery equivalent circuits and filtering algorithms. In [10], twelve kinds of battery equivalent circuits are introduced to simulate the charging and discharging process of the battery. Recently, fractional-order models (FOMs) have attracted growing attention in the arena of batteries [11], [12]. Different kinds of filtering algorithms including Luenberger observer [13], sliding-mode observer [14], particle filter [15], Kalman filter (KF) and extended Kalman filter (EKF) [16] are used in SOC estimation based on ECMs. The accuracy of SOC estimation using above methods relies significantly on the parameters of ECMs. The accuracy of the parameter database needs to be updated due to the different working conditions and aging. Therefore, their improved algorithms, such as adaptive unscented Kalman filter (AUKF) [17], dual extended Kalman filter (DEKF) and joint extended Kalman filter (JEKF) are employed to keep the model update overtime [18]. However, these improved methods may cause heavy computational load for online application such as BMS. In addition, the parameter database should be obtained by numerous offline experiments which is a demanding and time-consuming task [19].

Considering the above mentioned circumstances, the recursive least squares (RLS) methods to ECMs are employed because there is no matrix inversion required which is an advantage of RLS over KF and its variants [18]. Bastawrous proposed an adaptive forgetting factors recursive least-squares for $LiFePO_4$ battery [20]. Hu proposed a two-timescale scheme that estimates separately the battery fast dynamics (FD) and slow dynamics (SD) parameters [21]. Wei proposed a multi-timescale estimator to identify the ECM parameters and the battery open circuit voltage (OCV) in real time [22]. Dai suggested a different method to estimate the battery FD and SD on separated time scales [23]. Zhang employed a decoupled least squares, which shows better performance than conventional methods [24]. However, there is a lack of studies on the application of RLS and its variants to deep-discharging (DOD>85%) Li-ion battery. In addition, the effectiveness of the algorithms under different temperatures and working conditions including frequent speed changes, cruising uniform driving, uniform acceleration and deceleration driving, which can be equivalent to pulse current, constant power current and ramp current step profile, respectively, remain to be studied.

This paper proposes a SOC estimation method using a novel partial adaptive forgetting factors least square (PAFFRLS), which improves the dynamic tracking accuracy of parameters in the ECM. The proposed method adjusts the forgetting factors based on the own physical properties of each parameter in the ECM to accommodate to greatly changing of the parameters under deep-discharging range and highly dynamic working conditions. Gain matrix in the proposed method is split to update independently according to each parameter, which reduces the computational load caused by adaptive process of forgetting factors. In addition, the effectiveness of the proposed method under different temperatures and working conditions is examined based on numerous simulations and experiments.

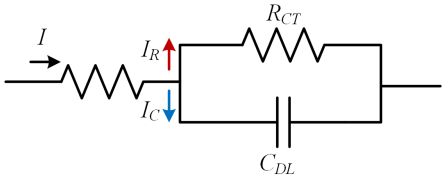

FIGURE 1. Simplified equivalent circuit.

ECMs for deep-discharging Li-ion batteries are analyzed in Section 2. Section 3 illustrates the PAFFRLS method in details. Four different working conditions and numerous experiments are shown in Section 4. Section 5 shows the result and discussion. The conclusions are given in Section 6.

II. BATTERY MODELING

A. EQUIVALENT CIRCUIT MODEL

A charge region is formed in the electrode and the electrolyte during the charging and discharging process. The voltage of the battery electrode directly affects the amount of charge in the region. The above reaction is similar to a capacitor, and the effect is called electrochemical charge transfer reaction. The electrochemical charge transfer reaction is mainly described by charge transfer over-potential, which can be described as Fig.1 in an equivalent circuit. A charge transfer resistance R_{CT} and a capacitor C_{DL} are employed to display the charge transfer over-potential. The resistance of the electrolyte and active mass is described as R_b [25]. R_{CT} and C_{DL} are two parameters that vary with SOC, aging degree and operating conditions according to the electrochemical theory. The internal resistance R_b is mainly affected by the aging degree of the battery.

Some common used ECMs have been proposed based on above theory. It mainly includes Rint model, Thevenin model, and *n-RC* model. The above ECMs are commonly consist of a voltage source (U_{oc}) describing the battery energy source and a resistor R_0 describing the internal resistance of the battery. The main purpose of using the above ECMs is to compute unobservable variables related to SOC and SOH such as OCV and internal resistance through the observable variables, such as terminal voltage and current during the working conditions. Fig.1 shows the general form of the ECMs. It is represented as a Rint model while $n = 0$. A circuit structure very similar to Fig.1, which simulates the dynamics of the charge and discharge of a battery from the perspective of electrochemical polarization by using a 1-*RC*

is used in the Thevenin model. The *n-RC* model simulates the concentration polarization by introducing multiple *RC* links to achieve accurate simulation of the dynamic process of the battery.

Transfer function of *n-RC* model in s-domain is described as equation (1):

$$G(s) = \frac{U_t(s) - U_{OC}(s)}{I(s)} = -(R_0 + \frac{R_{P1}}{1 + R_{P1}C_{P1}s} + ... + \frac{R_{Pn}}{1 + R_{Pn}C_{Pn}s}), \quad (n = 0, 1, 2, ...) \tag{1}$$

Taking the Thevenin model as an example, the circuit model parameters are derived as follows: The basic forward Euler transformation method in [20] is employed, which can decouple the parameters R_0 and U_{oc} from Equation (1). Equation (2) displays result in z-domain where Δt is sampling interval.

$$G(z) = -(\frac{a_0 + a_1 z^{-1}}{1 + a_2 z^{-1}}) \tag{2}$$

Equation (2) can be replaced by Equation (3) where a_1 to a_3 can be found in Equation (4).

$$U_k = a_0 I_k + a_1 I_{k-1} + a_2(U_{OC,k-1} - U_{k-1}) + U_{OC,k} \tag{3}$$

$$\begin{cases} a_0 = R_0 \\ a_1 = -R_0 + \dfrac{\Delta t}{C_P} + \dfrac{\Delta t R_0}{R_P C_P} \\ a_2 = \dfrac{R_0}{R_P C_P} - 1 \end{cases} \tag{4}$$

Equation (3) can be described as follows.

$$U_k = \phi_k \cdot \theta_k \tag{5}$$

where φ_k represents the data matrix as well as θ represents the parameter matrix of the system.

$$\phi_k = \begin{bmatrix} I_k & I_{k-1} & (U_{OC,k-1} - U_{k-1}) & 1 \end{bmatrix} \tag{6}$$

$$\theta_k = \begin{bmatrix} a_0 & a_1 & a_2 & U_{OC} \end{bmatrix}^T \tag{7}$$

B. MODEL SIMULATIONS AND ANALYSIS

The simulation accuracy of the above model for dynamic short pulses has been compared in [26]. This paper focuses on the simulation accuracy of various circuit models during deep-discharging process. Therefore, the following test steps are taken. Test bench and batteries specifications are described in details in Section 4:

a) The battery is rest for 1 hour while SOC is 15%, 10%, and 5%.

b) A discharge pulse with 10 seconds and 1C is employed.

c) Terminal voltage of the battery is measured.

d) Establish a terminal voltage tracking model for different circuit models using Simpowersystems in Matlab.

e) Change the discharge rate to 2.5C and 4C, and repeat steps (a) to (d).

The terminal voltage tracking results are shown in Fig. 3 (a)-(c). Table 1-3 show the terminal voltage tracking

TABLE 1. Results for equivalent circuit model analysis (rate = 1C).

Error (mV)	SOC=5%		SOC=10%		SOC=15%	
	Avg	Peak	Avg	Peak	Avg	Peak
Rint model	13.9	42.2	10.2	23.5	8.5	17.5
Thevenin model	2.7	10.3	1.7	5.0	1.5	3.3
2-RC model	2.2	5.3	1.4	2.7	1.3	1.7
3-RC model	2.6	6.4	1.6	3.0	1.3	1.7

TABLE 2. Results for equivalent circuit model analysis (rate = 2.5C).

Error (mV)	SOC=5%		SOC=10%		SOC=15%	
	Avg	Peak	Avg	Peak	Avg	Peak
Rint model	47.2	126.4	27.1	64.6	22.1	46.0
Thevenin model	10.7	33.7	4.6	10.5	3.5	7.6
2-RC model	10.4	27.2	4.4	8.2	3.1	4.7
3-RC model	11.5	30.1	5.3	9.9	3.5	6.5

TABLE 3. Results for equivalent circuit model analysis (rate = 4C).

Error (mV)	SOC=5%		SOC=10%		SOC=15%	
	Avg	Peak	Avg	Peak	Avg	Peak
Rint model	96.0	305.2	48.7	152.5	36.3	84.3
Thevenin model	25.6	70.6	12.9	35.1	6.9	16.0
2-RC model	25.4	58.6	12.7	28.3	6.8	11.3
3-RC model	26.2	67.4	13.1	34.7	7.7	14.9

average error and peak error of the four mentioned ECMs including Rint model, Thevenin model, 2-*RC* model and 3-*RC* model.

Table 1-3 indicate that the maximum tracking error of the Rint model is 305.2mV, which shows weak ability to track dynamic current profiles. The 2-*RC* model displays minimum terminal voltage tracking error compared with others. The minimum and maximum peak error are 1.7 mV and 58.6mV, respectively. The tracking error of the 3-*RC* model is slightly higher than the 2-*RC* model, however it is not suitable for the EVs because of the higher computational load. The minimum and maximum peak error of Thevenin model are 3.3 mV and 70.6mV, respectively. The average error is close to the 2-*RC* model under different discharge rates. Therefore, the Thevenin model is more suitable for the practical application of BMS within the error tolerance as for the smaller computation load than *n-RC* model, which is employed in this paper.

In addition, table 1-3 indicate that the tracking performance of the mentioned ECMs on terminal voltage is significantly weakened as the SOC decreases from 15% to 5%. Taking the 2-RC model with the best tracking performance at 4C rate as an example, the average error of the terminal voltage tracking is 6.8mV and the peak error is 11.3mV while SOC is 15%. The average error increases to 25.4 mV and the peak error is 58.6 mV which shows an 8.6-fold increase while SOC is 5%. In addition, as the discharge rate increases, the tracking performance is significantly weakened at the

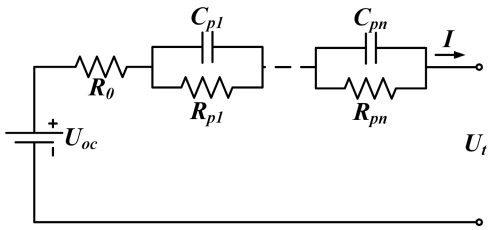

FIGURE 2. Battery equivalent circuit model.

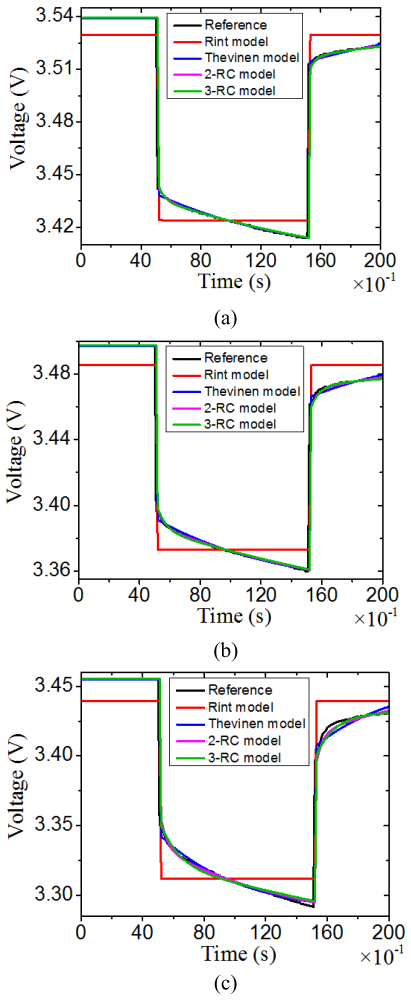

FIGURE 3. Simulation results under 1C rate: (a) SOC = 15% and (b) SOC = 10% (c) SOC = 5%.

same SOC range. Taking the 2-RC model with the best tracking accuracy while SOC is 5% as an example, the average and peak error are 2.2mV and 5.3mV under 1C rate, respectively. The average and peak error are 25.4 mV and 58.6mV under 4C rate. The tracking peak error shows a 11.6-fold increase. As can be clearly seen in above model simulations and analysis, the physical property parameters of the Li-ion battery change greatly while the DOD is high. Thus, the tracking of the terminal voltage is greatly affected by the dynamic parameters under high rate and DOD, which leads to a large tracking error using the conventional time domain methods.

Given the above simulations and analysis, a novel PAFFRLSis proposed to meet the issues. The proposed method adjusts the forgetting factors based on the own physical properties of each parameter in the ECM to accommodate to greatly changing of the parameters under deep-discharging range and highly dynamic working conditions.

III. ONLINE SOC ESTIMATION METHOD

The parameters in ECMs can be calculated offline after testing at different temperatures, discharge rates and SOCs, based on the conventional method described in Section 2. A comprehensive database of battery parameters can be obtained through a large number of tests. However, it is difficult to fully simulate all the conditions in the actual operation of EVs. In addition, the accuracy based on offline parameters calculation is not reliable enough under high discharge rate and DOD according to the analysis in section 2. Thus, there is often a certain deviation in actual working conditions. On the other hand, the parameters in battery ECMs will change with the temperatures, working conditions, SOCs, and aging in the actual operation of the EVs. Therefore, the parameters should be updated online. In order to solve the above issues, this paper proposes a PAFFRLSmethod to accurately identify the parameters in the battery ECM on line.

A. RECURSIVE LEAST SQUARE WITH FORGETTING FACTORS

In conventional least square estimation theory, unknown parameters are chosen in such a way which the sum of the squares of the difference between the actually observed and the computed values is a minimum [27].

$$J = \sum_{i=1}^{n} [y(i) - \phi(i)\hat{\theta}(i)]^2 \tag{8}$$

The conventional (RLS) estimation can be described as follow:

$$K(k) = \frac{P(k-1)\cdot\phi(k)}{1+\phi^T(k)\cdot P(k-1)\cdot\phi(k)} \tag{9}$$

$$P(k) = (1 - K(k)\cdot\phi^T(k))P(k-1) \tag{10}$$

$$\theta(k) = \theta(k-1) + K(k)(y(k) - \phi^T(k)\cdot\theta(k-1)) \tag{11}$$

where P is the covariance matrix and K is referred to as the update gain.

The periodic resetting of the estimation scheme can potentially capture the new values of the parameters. The model will lose the ability to track slow changes in parameters while the covariance matrix decays to around zero. The concept of forgetting factors has been proposed which can be viewed as giving less weight to older data and more weight to recent data. The single fixed forgetting factors is not able to track parameters with different variation rates. Thus, a method called self-turning regulars with multiple forgetting factors has been widely used in the field of control [28]. The P can

be described as equation (11) and A is the multiple forgetting factors matrix.

$$P(k) = A^{-1}[I - K(k)\phi^T(k)P(k-1)]A^{-1} \quad (12)$$

$$A = diag[\lambda_1\ \lambda_2\ \lambda_3\ \lambda_4] \quad (13)$$

B. PARTIAL ADAPTIVE FORGETTING FACTOR RLS (PAFFRLS)

Parameters in ECMs including R_0, U_{oc}, R_p and C_p vary with different rates under the whole working condition. Taking the dynamic working condition as an example, the C_p and R_p show large fluctuations with the dynamic input profile. On the contrary, R_0 and U_{oc} change with SOC, which show a time integral of input profile. Additionally, there is not a significant change throughout the discharge process but a significant increase while the DOD is high. Therefore, the following issues should be solved when estimating the parameters of deep-discharging Li-ion batteries.

(a) The error sources of each parameter in the ECM are different and the changes of the errors are asynchronous. Thus, the error of each parameter should be tracked independently in the recursive solution process.

(b) The parameters vary with different rates due to their own physical characteristics. Therefore, the forgetting process of the algorithm should be able to track each parameter with different time-varying rates.

However, in conventional methods, equation (8) - (10) indicate that the covariance is a scalar which is superimposed by all parameter errors. Therefore, the algorithm may lose the ability to track all parameters while the error is caused by the errors of partial parameters. For instance, if there are drifts in R_p and C_p because of the dynamic current profile, the same order will be applied to R_0 and U_{oc} which results in unnecessary corrections since the R_0 is proved to show a slow change process under the whole working condition. Thus, a decoupling method is employed in this paper to track the error of each parameter independently.

The error of the proposed PAFFRLS method is defined as shown in Equation (14), which can be regarded as a separate form of the equation (8).

$$\begin{aligned} J = &\sum_{i=1}^{k} \lambda_1^{k-i}[y(i) - \phi_1(i)\hat{\theta}_1(i) - \sum_{m=2,3,4} \phi_m(i)\theta_m(i)]^2 \\ &+ \sum_{i=1}^{k} \lambda_2^{k-i}[y(i) - \phi_2(i)\hat{\theta}_2(i) - \sum_{m=1,3,4} \phi_m(i)\theta_m(i)]^2 \\ &+ \sum_{i=1}^{k} \lambda_3^{k-i}[y(i) - \phi_3(i)\hat{\theta}_3(i) - \sum_{m=1,2,4} \phi_m(i)\theta_m(i)]^2 \\ &+ \sum_{i=1}^{k} \lambda_4^{k-i}[y(i) - \phi_4(i)\hat{\theta}_4(i) - \sum_{m=1,2,3} \phi_m(i)\theta_m(i)]^2 \end{aligned} \quad (14)$$

The recursive equations of θ_1 after separation is shown in equation (15) - (17).

$$K_1(k) = \frac{P_1(k-1)\phi_1(k)}{\lambda_1 + \phi_1^T(k)P_1(k-1)\phi_1(k)} \quad (15)$$

$$P_1(k) = (I - K_1(k)\phi_1^T(k))P_1(k-1)\frac{1}{\lambda_1} \quad (16)$$

$$\begin{aligned} \hat{\theta}_1(k) = &\hat{\theta}_1(k-1) + K_1(k)(y(k) \\ &-\phi_1(k)\hat{\theta}_1(k-1) - \sum_{m=2,3,4} \phi_m(k)\theta_m(k)) \end{aligned} \quad (17)$$

$\theta_m(k)$ (m = 2, 3, 4) in equation (17) are unknown. According to the assumption in [29], the substitution is also justified when the actual and estimated values are very close to each other or within the algorithm region of convergence. Thus, the $\theta_m(k)$ (m = 2, 3, 4) are replaced by their estimates, upon the substitution, the recursive equation is shown in equation (18).

$$\begin{aligned} &\hat{\theta}_1(k) + K_1(k) \sum_{m=2,3,4} \phi_m(k)\hat{\theta}_m(k) \\ &\quad = \hat{\theta}_1(k-1) + K_1(k)(y(k) - \phi_1(k)\hat{\theta}_1(k-1)) \end{aligned} \quad (18)$$

The recursive forms of θ_2, θ_3 and θ_4 are similar with equation (18). Thus, the recursive equation of the proposed PAFFRLS is shown as follows.

$$\hat{\theta}(k) = \hat{\theta}(k-1) + K(k)(y(k) - \phi^T(k)\hat{\theta}(k-1)) \quad (19)$$

$$K(k) = \begin{bmatrix} P_1(k-1)\phi_1(k)/(\lambda_1(1+S(k))) \\ P_2(k-1)\phi_2(k)/(\lambda_2(1+S(k))) \\ P_3(k-1)\phi_3(k)/(\lambda_3(1+S(k))) \\ P_4(k-1)\phi_4(k)/(\lambda_4(1+S(k))) \end{bmatrix} \quad (20)$$

where

$$S(k) = \sum_{i=1}^{4} \frac{P_i(k-1)\phi_i(k)^2}{\lambda_i} \quad (21)$$

As can be clearly seen from Equation (19) - (20) that the decoupled recursive gain K can be updated according to the independent error generated by each parameter without affecting each other. Further, each parameter can be tracked with different rates by using four separate independent forgetting factors.

However, the physical characteristics of each parameter should be considered when confirming the value of each parameter. Parameters in the battery ECM are not all physical quantities that the practical significance for them can be found. The U_{oc} and R_0 are the inherent electrical parameters in batteries which do not change with the external working conditions. As for U_{oc}, there is a one-to-one correspondence between U_{oc} and SOC as well as the SOC is related to the embedding quantity of lithium-ion in the active material and with static thermodynamics [30]. The internal resistance R_0 and SOC exhibits a parabolic-like relationship, which means that the internal resistance is significantly higher than the plateau while the SOC is high and low. On the contrary, R_p and C_p characterize the electrochemical polarization which

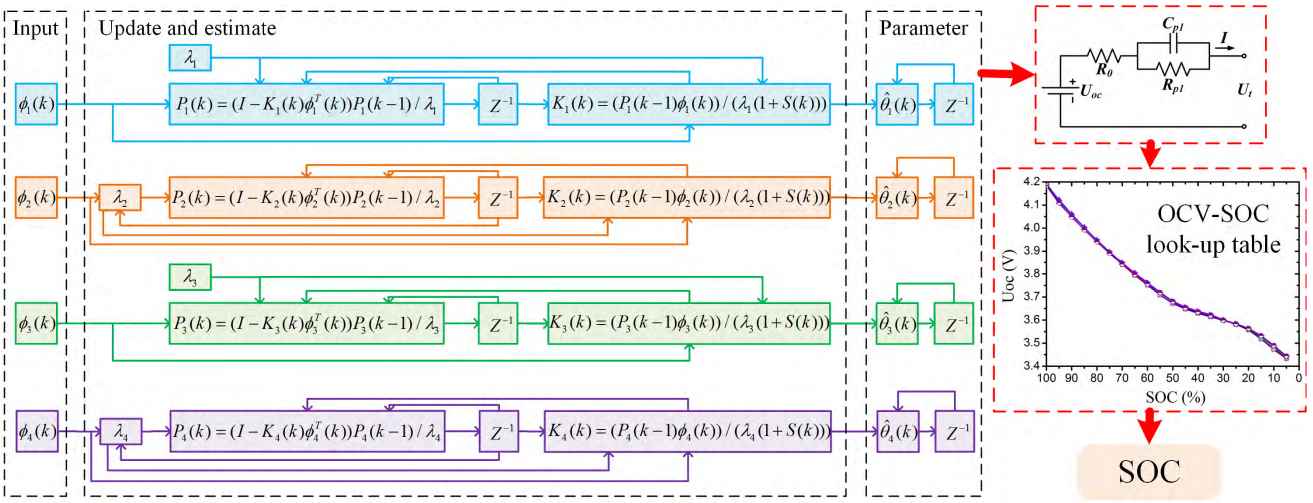

FIGURE 4. Steps of PAFFRLS.

vary with the working conditions a lot, especially the dynamic pulse profile is employed.

$$\begin{cases} \lambda_1(k) = \xi_1 \\ \lambda_2(k) = 1 - 1/(1 + \dfrac{\xi_2}{\phi^T(k)P_2(k-1)\phi(k)}) \\ \lambda_3(k) = \xi_3 \\ \lambda_4(k) = 1 - 1/(1 + \dfrac{\xi_4}{\phi^T(k)P_4(k-1)\phi(k)}) \end{cases} \tag{22}$$

In order to track each parameter according to its own characteristics, a partial adaptive method for forgetting factors is employed in this paper. Equation (22) indicates the partial adaptive forgetting factors matrix consist of two adaptive forgetting factors based on inputs and two fixed forgetting factors for R_0 and U_{oc}, which are assigned to a_1, a_2, a_0 and U_{oc} in Equation (7), respectively. The adaptive equations in [20] are used and the fixed forgetting factors are determined by genetic algorithms.

The partial adaptive forgetting factors in Equation (22) not only adjust variation inputs, but also track the variation of battery parameters dynamically, which improve the tracking effect of the system. The accuracy of tracked U_{oc} based on this method is shown in section 5. Steps of SOC estimation using the proposed PAFFRLS are shown in Fig. 4.

IV. EXPERIMENTS

The battery test bench, which composes of a battery tester (Neware BTS-4000-10V/10A) for loading and sampling the battery, a host computer with Neware Software for on-line experiment control and data recording, a HIOKI BT3563 battery tester for internal resistance measurement, and a thermostat for controlling test temperature, is shown in Fig. 5.

The cylindrical Li(NiCoMn)O_2 (NCM) batteries, are employed in the tests, and the specifications are shown in Table 4. The tests are carried out at different temperatures of −15°C, −5°C, 5°C, 10°C, 15°C, 25°C and 35°C, respectively.

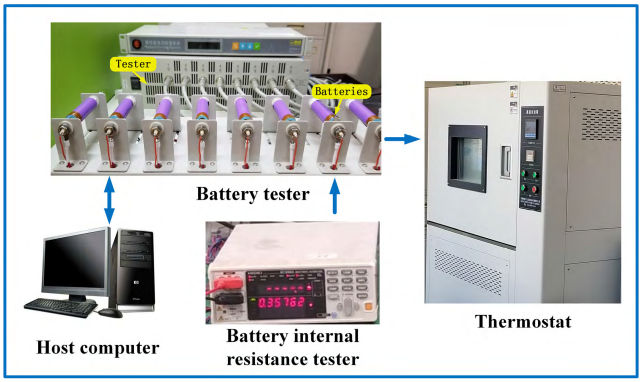

FIGURE 5. Battery test bench.

TABLE 4. Battery specifications at 25°C.

Type	Size	Terminal voltage (V)	Operating voltage (V)	Capacity (Ah)	Maximum discharge rate (C)
NCM	18650	3.7	2.7-4.2	2.5	4

A. STATIC CAPACITY TEST

The capacity of the test cells used in this paper are statically calibrated as follows:

a) The battery is fully charged by constant-current constant-voltage (CC-CV).

b) Discharge at 1C rate to cutoff voltage.

c) Repeat the above process 3 times and take the average of three test capacity as the initial capacity.

B. HYBRID PULSE TEST (HPT)

Hybrid Pulse Power Characterization (HPPC) Test is intended to determine dynamic power capability over the

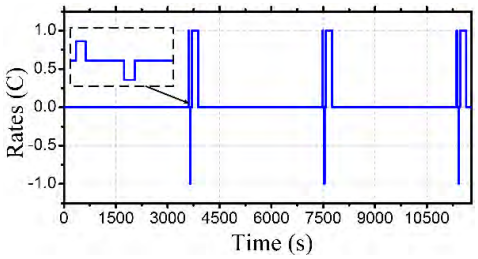

FIGURE 6. HPT test profile.

TABLE 5. Test profile.

Time Increment (s)	Cumulative Time (s)	Rates (C)
10	10	1
40	50	0
10	60	-1
40	100	0
180	280	1
3600	3780	0

device's useable charge and voltage range using a test profile that incorporates both discharge and regen pulses [31].

Test profile in this paper is similar to the HPPC Test to validate the proposed PAFFRLS method and correct the OCV-SOC look-up table given by the manufacturer. The test profile in this paper is shown in Table 5 and Fig. 6.

In each HPT test cycle, a 10s charge and discharge pulse, a CC discharge process, and a long period of rest are included. Among them, the 10s short pulse is used to accurately calculate the U_{oc} and ECM parameters according to the terminal voltage at each SOC range. The CC discharge process is employed to fix the discharge capacity to reach the next SOC range by setting the discharge current and time. Since the U_{oc} can not be measured during the test, the terminal voltage after a long time rest is measured at each SOC level, which is used as the reference U_{oc} at each SOC range to verify the U_{oc} estimation accuracy using the 10s pulse.

Therefore, the reference and calculated U_{oc} at each SOC range can be obtained through the HPT test.

C. WORKING CONDITIONS TEST

The typical working conditions of EVs mainly includes: frequent acceleration and deceleration in cities, smooth acceleration or deceleration or uniform speed in suburb or highway. Thus, the SOC estimation methods employed in EVs need to show higher estimation accuracy under different working conditions. The typical test working conditions provided by USABC, UN/ECE, and EPA organizations are used to verify the estimation accuracy of the proposed PAFFRLS method, including Dynamic Stress Test (DST), Urban Dynamometer Driving Schedule (UDDS), US06, UN/ECE Extra-Urban Driving Cycle (EUDC) in this paper.

DST is a simplified working condition of EVs which can effectively simulate dynamic discharging. The 360 seconds DST test profiles are repeated end-to-end with no time delay

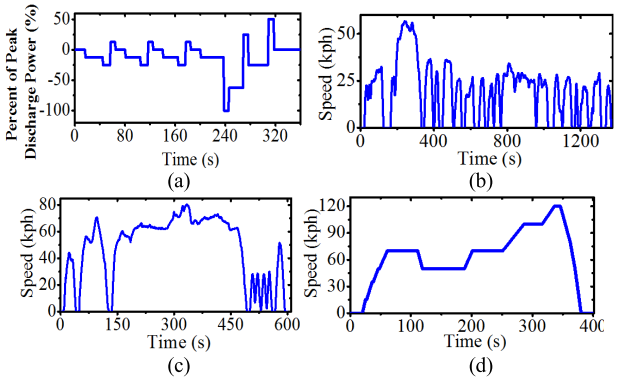

FIGURE 7. Working conditions: (a) DST (b) UDDS (c) US06 and (d) EUDC.

(rest period) which is shown in Fig. 7 (a) [32]. Fig.7 (a) displays that DST working condition contains short pulses of different magnifications in the 360s cycle, which is a simulation case similar to the pulse test used in the second section of this paper.

However, the current change is not composed of regular short pulses during the actual working condition of EVs. Other three typical working conditions are shown in Fig.7 (b)-(d). The EPA UDDS is commonly called the "LA4" or "the city test" and represents city driving conditions. The US06 is a high acceleration aggressive driving schedule that is often identified as the "Supplemental FTP" driving schedule. The UN/ECE Extra-Urban Driving Cycle (EUDC) is Part 2 of the ECE Type 1 Test.

A method for the battery current computation based on the speed is given in [32], as shown in Equation (16)-(17) and all coefficients of a reference electric car are shown in the table 6.

$$P_t = (M \cdot g \cdot f + \frac{1}{2}\rho_a \cdot C_D \cdot A_f \cdot v^2 + M \cdot \delta \cdot \dot{v} + M \cdot g \cdot i)v \quad (23)$$

$$I_b = -(\frac{1}{\eta_w}\frac{1+sgn(P_t)}{2} + \eta_r \frac{1-sgn(P_t}{2})\frac{P_t}{\alpha \cdot N \cdot V_b} \quad (24)$$

V. RESULT AND DISSCUSSION

The basis for batteries SOC estimation is accurate OCV-SOC look-up tables and U_{oc} in real time, which is verified in this section.

Different charge and discharge pulses (± 0.5, ± 1, ± 1.5, ± 2, ± 2.5, ± 3, ± 3.5 and ± 4) are employed in the HPT test for NCM cells. The test cells in this section are grouped according to capacity deviation, which is less than 1%. 8 cells are divided into one group and the test result is the average of 8 cells.

A. OCV-SOC LOOK-UP TABLE CORRECTION

OCV-SOC look-up table correlation is significant. The U_{oc} which can be observed in rest steps during different rates HPT test are displayed in Fig. 8.

TABLE 6. Reference electric car parameters [32], [33].

Symbol	Description	Value
M	Vehicle mass with passengers (kg)	1600
g	Gravity acceleration (ms^{-2})	9.81
ρ_a	Air density (kgm^{-3})	1.225
A_f	Front area (m^{-2})	2.1
C_D	Aerodynamic drag coefficient	0.3
f_r	Rolling resistance coefficient	0.005
δ	Rotational inertia factor	1.05
i	Grade of road	0
V_b	Battery working voltage (V)	3.3
N	Number of batteries	40
α	Scaling factor	2.5
η_w	Efficiency from battery to wheel	0.7
η_r	Efficiency from wheel to battery	0.3

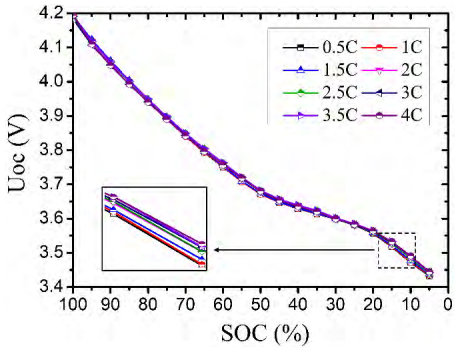

FIGURE 8. OCV-SOC look-up table correlation.

Fig. 8 indicates that the test cells shows a voltage platform while SOC range is 20%-50%. The largest deviation between OCV-SOC curves of different discharge rates is 0.36% as well as the curves of high rate groups are higher than the curves of low rates group in Fig. 8 due to the no complete polarization reaction. An average OCV-SOC look-up table is employed to avoid the issues above.

As can be clearly seen in Fig. 8 that the OCV-SOC look-up table of NCM batteries is steeper than $LiFePO_4$ (LFP) batteries, which makes estimating SOC through the OCV-SOC look-up table a viable method. However, the OCV can not be directly measured during working conditions, which can only be read after a long time rest. In addition, OCV is affected by the length of the rest time. Although the terminal voltage (U_t) of the battery can be measured during working conditions, U_t does not show a fixed correspondence with SOC. This is because the U_t at the same SOC range is affected by the temperatures, working conditions, and aging conditions.

Therefore, the steps in Fig. 4 are employed to solve the above issues. The U_{oc} under the entire working condition is accurately estimated online using the proposed PAFFRLS method, as well as the corrected OCV-SOC look-up table in this section is applied to estimate the SOC.

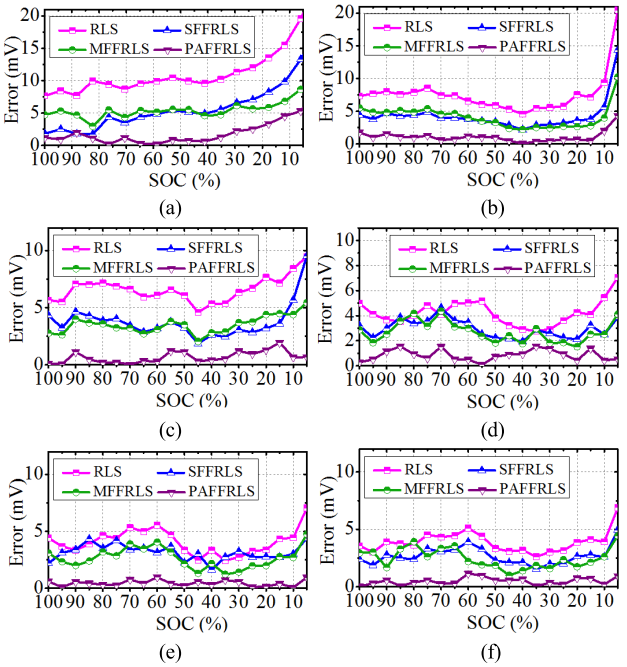

FIGURE 9. Error of U_{oc} estimation, Rate = 1C: (a) −15°C (b) −5°C (c) 5°C (d) 15°C (e) 25°C and (f) 35°C.

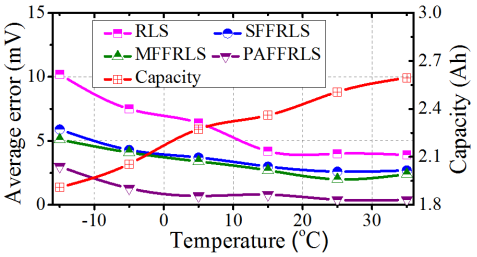

FIGURE 10. Average error of U_{oc} estimation and capacity at different temperatures.

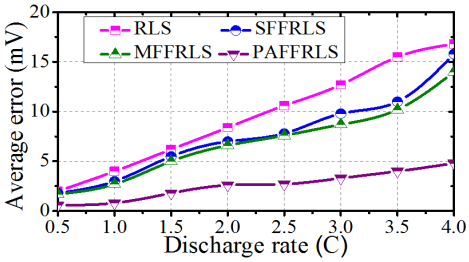

FIGURE 11. Average error of different parameters estimation methods under different discharge rates. T = 15°C.

B. U_{oc} ESTIMATION WITH PAFFRLS UNDER HPT TEST

U_{oc} is the most important parameter in the ECM while SOC estimation because there is a one-to-one correspondence between U_{oc} and SOC. Thus, the U_{oc} estimation accuracy of the proposed PAFFRLS is verified under different temperatures and discharge rates.

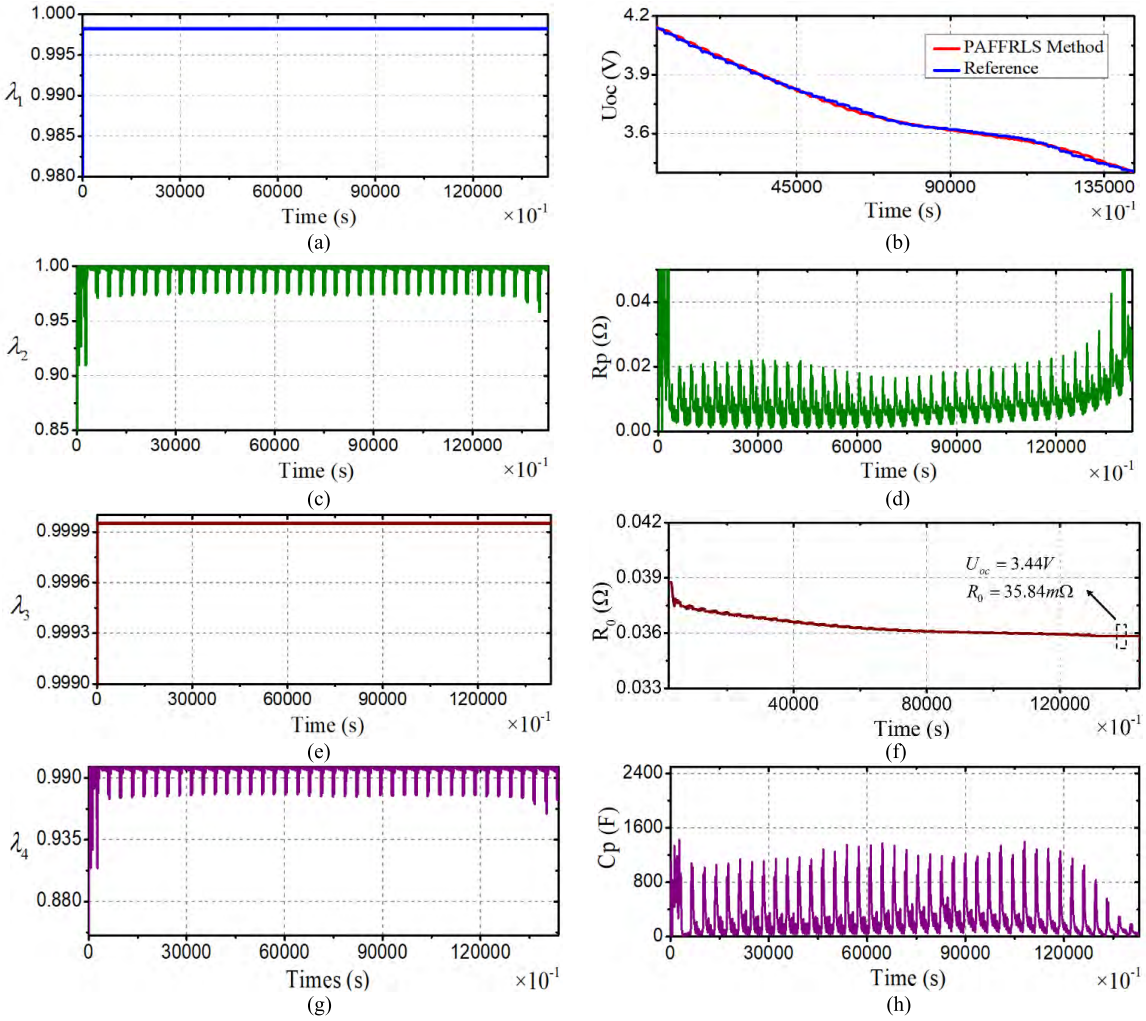

FIGURE 12. Results of NCM cell parameters estimation. T = 15°C.

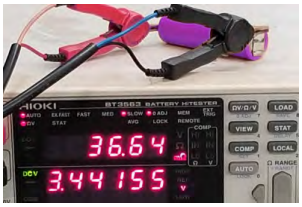

FIGURE 13. Results of internal resistance measurement. T = 15°C.

The conventional RLS, single forgetting factors RLS (SFFRLS) and multiple forgetting factors RLS (MFFRLS) are used to compare with PAFFRLS method to verify the accuracy of the U_{oc} estimation. The reference U_{oc} is described as follows: the terminal voltage after an hour rest in HPT test is employed as the reference U_{oc}.

Fig. 9 (a)-(f) indicate that the proposed PAFFRLS shows better accuracy compared to the other three methods over the entire SOC ranges. As can be clearly seen in Fig.9, estimation accuracies of three conventional methods are significantly reduced as well as the proposed PAFFRLS still shows good performance on deep-discharging process (DOD>85%) at different temperatures. The U_{oc} estimation errors at −15°C, −5°C, 5°C, 10°C, 15°C, 25°C and 35°C are 5.3mV, 4.3mV, 0.7mV, 0.5mV, 1mV and 0.9mV, respectively, while SOC is 5%.

This is because when the DOD is high, the internal resistance R_0 and polarization resistance R_p become larger, resulting in more severe fluctuations in the terminal voltage under the same current profile. However, all parameters in ECM are applied with a same gain matrix while the three conventional RLS methods are employed, which results in some parameters that should have less error are also applied with the same overall error. On the contrary, the proposed PAFFRLS realizes independent tracking of each parameter by decoupling the gain matrix, so that each parameter can be recursed according to its own estimation error, which shows better effect at high DOD.

In addition, Fig. 10 indicates that as the temperature decreases, the internal resistance under low temperature will

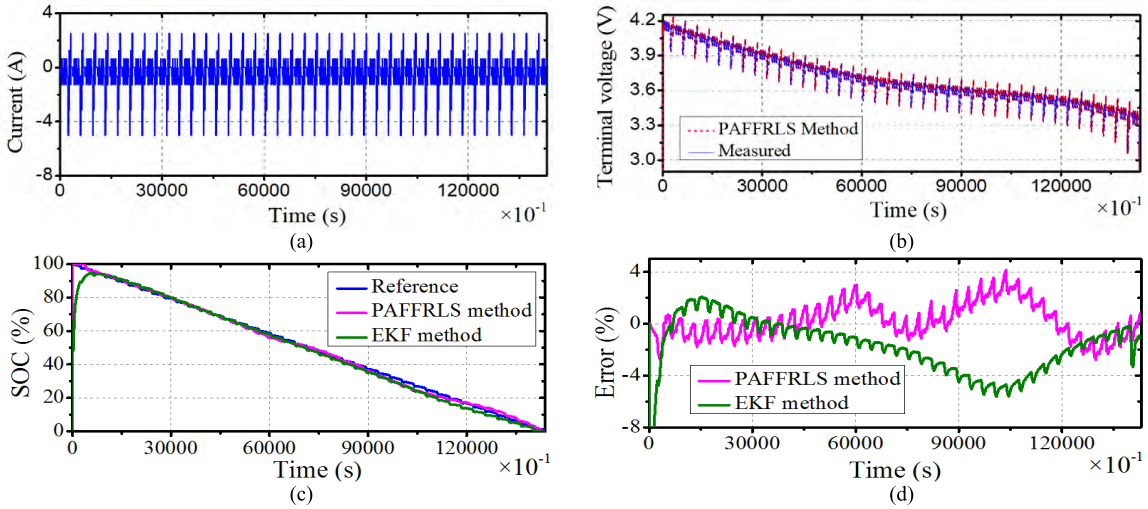

FIGURE 14. Result of NCM cells SOC estimation under DST working condition. T = 15°C.

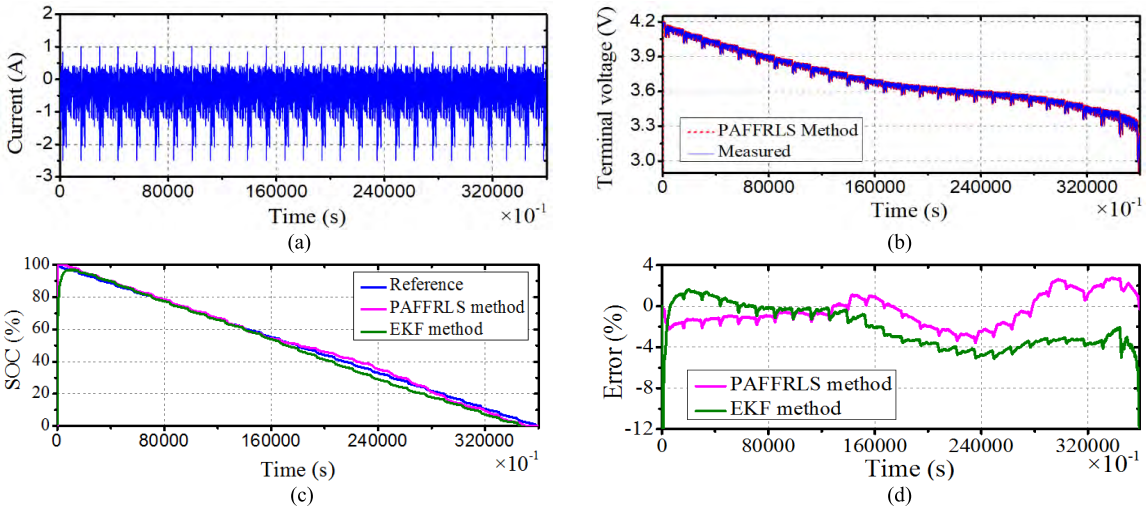

FIGURE 15. Result of NCM cells SOC estimation under UDDS working condition. T = 15°C.

become larger, resulting in an increase in the error of U_{oc} estimation using mentioned methods. The U_{oc} estimation average errors using the proposed PAFFRLS at −15°C, −5°C, 5°C, 10°C, 15°C, 25°C and 35°C are 3.0mV, 1.3mV, 0.7mV, 0.8mV, 0.4mV and 0.4mV, respectively, which show good performance at different temperatures.

Results of the HPT test with different rates including RLS, SFFRLS, MFFRLS and PAFFRLS method are shown in Fig. 11. Fig. 11 indicates that errors of the proposed PAFFRLS method are all below 5 mV at 15°C while discharge rates are different. Moreover, U_{oc} estimation errors of four methods increase with the increase of discharge pulses rates. It is because that the discharging process of polarization capacitor in the ECM cannot be fully performed during a short period of rest while the pulses in HPT are large, which reduces the simulation accuracy of the ECM on the discharge and charge process of cells.

C. PARAMETERS ESTIMATION UNDER DST WORKING CONDITION

DST working condition is used to verify cells SOC estimation in this section. The proposed PAFFRLS is employed to estimate U_{oc} online and the corrected OCV-SOC look-up table in Fig. 8 is then used to estimate SOC. The results of parameters estimation are shown in Fig. 12.

Fig.12 (a), (c), (e) and (g) display the forgetting factors of U_{oc}, R_p, R_0 and C_p, respectively. λ_1 and λ_3 are 0.9982 and 0.9995 in this paper while DST condition is used. λ_2 and λ_4 are adaptive based on the current change. Smaller forgetting factors (λ_2 and λ_4) are obtained in the system while the current changes greatly to enhance the ability to track dynamic parameters. Fig. 12 (b) displays the U_{oc} estimation error is less than 8mV while DST working condition is used. The reference U_{oc} in Fig. 12 (b) is based on the actual SOC and the

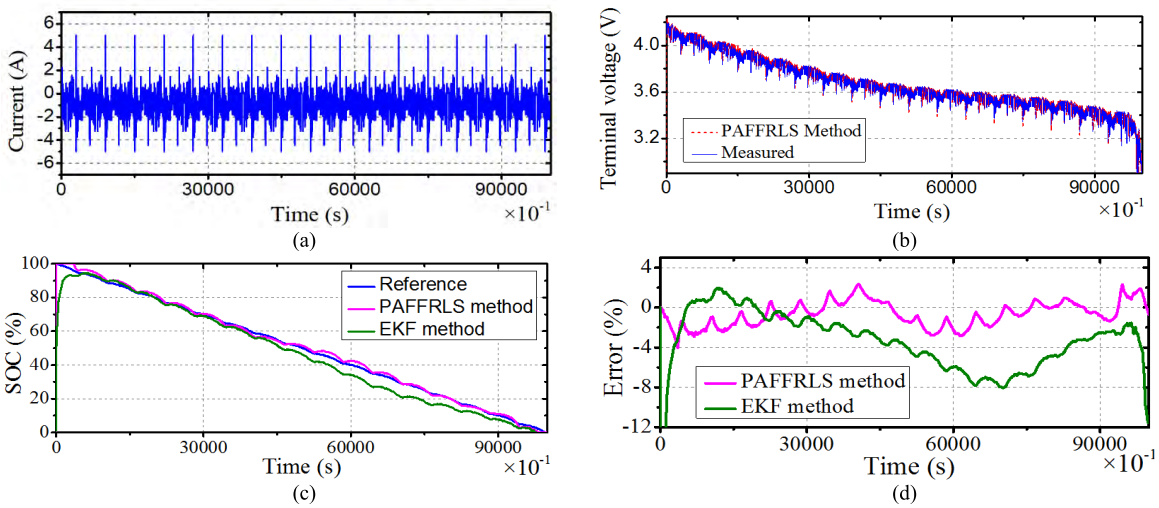

FIGURE 16. Result of NCM cells SOC estimation under US06 working condition. T = 15°C.

corrected look-up table in Fig. 8 on the basis of the accurate current measurement.

R_0 in Fig. 12 (f) is almost a constant at a value of 36 mΩ, which is consistent with the measurement result of the internal resistance tester in Fig.13. Fig. 12 (d) and (h) display R_p and C_p respectively which follow the inputs change. Both R_p and C_p have larger values while the operating condition is at a large rate discharge pulse, so that the time constant in equivalent circuit is larger, which is similar to Fig. 11.

D. SOC ESTIMATION UNDER DIFFERENT WORKING CONDITIONS

In this paper, the commonly used EKF method in BMS and the proposed PAFFRLS method are used to estimate the SOC of NCM batteries under different working conditions. The ECM parameters in EKF are calculated based on the offline method in section 2. Four different working conditions, including DST, UDDS, US06 and EUDC are used to verify the applicability of the proposed PAFFRLS method.

The estimation result of DST working condition is shown in Fig. 14. As can be clearly seen in Fig.14 (b), the terminal voltage is tracked accurately during the whole dynamic current profile in Fig. 14 (a). Fig. 14 (c) indicates there is a good fitness of SOC estimation using the proposed PAFFRLS method. The average errors of PAFFRLS and EKF are 1.11% and 1.90%, respectively. The errors of the SOC estimation are displayed in Fig. 14 (d). Based on the DST working condition test, the proposed PAFFRLS method shows good performance on the NCM cells SOC estimation.

The results of the UDDS and US06 working conditions are shown in Fig. 15 (a)-(d) and Fig. 16 (a)-(d), respectively. Fig. 15 (a) and Fig. 16 (a) display the current profiles of two working conditions, which are both more dynamic than the DST working condition. As can be clearly seen in Fig. 15 (b) and Fig. 16 (b), the terminal voltage is tracked accurately during the whole working conditions. Fig. 15 (c) and Fig. 16 (c) indicate good fitness of the estimated SOC by the proposed PAFFRLS method. The error of the SOC estimation is displayed in Fig. 15 (d) and Fig. 16 (d). As for UDDS working condition, the average errors of PAFFRLS and EKF are 1.25% and 2.76% respectively. The average errors of US06 working condition are 1.17% and 3.83% respectively.

TABLE 7. Error of SOC estimation.

Error (%)	DST	UDDS	US06	EUDC
Peak error	4.14	3.32	4.04	4.61
Average error	1.11	1.25	1.17	1.26

The result of the EUDC working condition is shown in Fig. 17 (a)-(d). Fig. 17 (a) displays the current profile of the working condition, which is less dynamic than the other three working conditions. As can be clearly seen in Fig. 18 (b), the terminal voltage is tracked accurately during the whole working condition. Fig. 17 (c) indicates that there is a good fitness of the SOC estimation using the proposed PAFFRLS method. The average errors of PAFFRLS and EKF are 1.26% and 2.84%, respectively. The error of the SOC estimation is displayed in Fig. 17 (d).

Table 7 displays the comparison of the SOC estimation results using the proposed PAFFRLS under mentioned working conditions. The peak errors are all less than 5% and the average errors are all less than 1.3%. As can be clearly seen in Fig. 14-17 (d) that the SOC estimation errors are larger and show fluctuations in the voltage platform, which is related to the inaccuracy of OCV-SOC look-up table in the platform period. In addition, the peak errors are all less than 3% while DOD are higher than 90%, which indicates that the proposed PAFFRLS shows better SOC estimation effect under high dynamic working conditions and high DOD.

Fig. 18 (a)-(d) show the SOC estimation results under UDDS working condition at different temperatures. As can

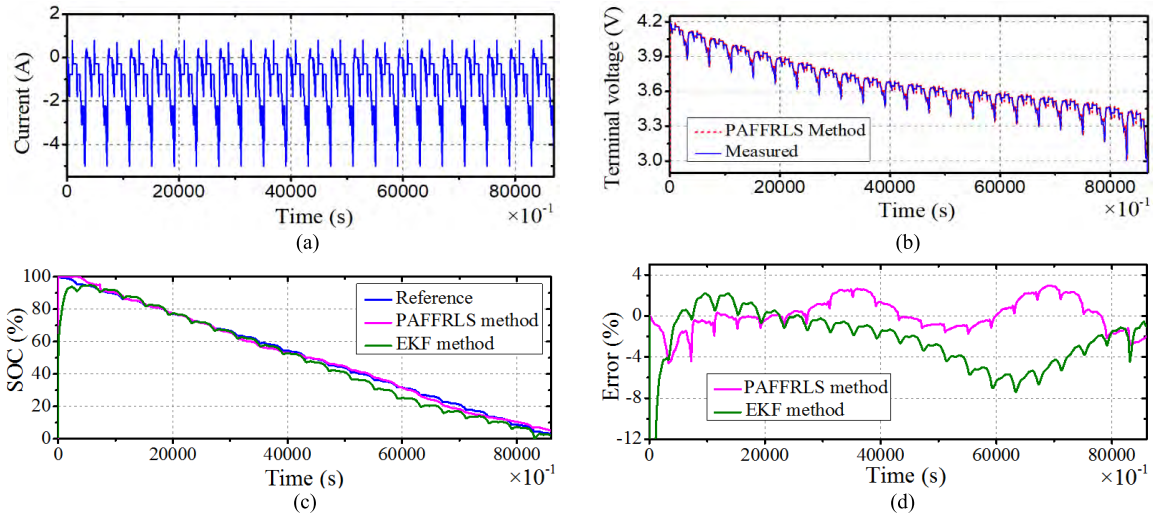

FIGURE 17. Result of NCM cells SOC estimation under EUDC working condition. T = 15°C.

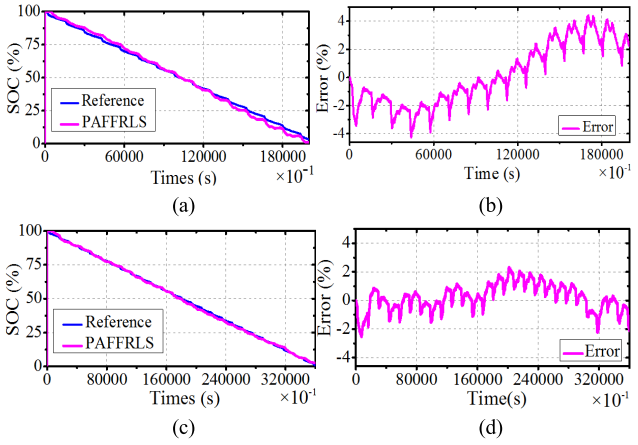

FIGURE 18. Result of NCM cells SOC estimation at different temperatures. (a)-(b): −15°C, (c)-(d): 35°C.

TABLE 8. Error of SOC estimation.

Error (%)	-15°C	15 °C	35°C
Peak error	4.43	3.32	2.55
Average error	1.91	1.25	0.92

be clearly seen in Table 8 that average errors are all less than 2% as well as peak errors are all less than 5%. However, as the temperature decreases, the error of SOC estimation by the PAFFRLS method increases. The method shows the largest error when the temperature is −15°C, which displays the same changes as Fig. 10. the peak error is 4.43% and average error is 1.91% at −15°C. Since the internal resistance of the battery at low temperature is large, especially while the DOD is high, which causes a steeper voltage change. Thus, the SOC estimation accuracy of the proposed PAFFRLS is degraded at low temperatures.

The applicability of the proposed method under different ECMs and combination working conditions will be studied in the future work.

VI. CONCLUSION

This paper proposes a SOC estimation method using a novelPAFFRLS, which improves the dynamic tracking accuracy of parameters. The proposed method adjusts the forgetting factors based on the own physical properties of each parameter in the ECM to accommodate to greatly changing of the parameters under deep-discharging range and highly dynamic working conditions. Gain matrix in the proposed method is split to update independently according to each parameter, which reduces the computational load caused by adaptive process of forgetting factors.

The validity of the PAFFRLS has been established with numerous experimental tests. The accuracy of parameters estimation in ECM is verified at different temperatures and different discharge rates. The accuracy of the proposed PAFFRLS for U_{oc} estimation is less than 3mV while the discharge rate is 1C and the temperature is within the temperature range of −15°C to 35°C. The error of internal resistance estimation is less than 1mΩ.

Furthermore, the average errors of the SOC estimation under four different kinds of working conditions including DST, UDDS, US06 and EUDC, are all less than 1.3% as well as the peak errors are all less than 5%. In addition, the peak errors are all less than 3% while the DOD are higher than 90%, which illustrates the effectiveness of the proposed method in the case of deep-discharging Li-ion battery.

The proposed PAFFRLS shows good performance on online deep-discharging Li-ion battery SOC estimation under complicated working conditions at different temperatures, which provides a better guidance to the design of BMSin EVs.

REFERENCES

[1] M. A. Hannan, M. S. H. Lipu, A. Hussain, M. H. Saad, and A. Ayob, "Neural network approach for estimating state of charge of lithium-ion battery using backtracking search algorithm," *IEEE Access*, vol. 6, pp. 10069–10079, 2018.

[2] X. Hu, C. Zou, C. Zhang, and Y. Li, "Technological developments in batteries: A survey of principal roles, types, and management needs," *IEEE Power Energy Mag.*, vol. 15, no. 5, pp. 20–31, Sep. 2017.

[3] X. Hu, H. Yuan, C. Zou, Z. Li, and L. Zhang, "Co-estimation of state of charge and state of health for lithium-ion batteries based on fractional-order calculus," *IEEE Trans. Veh. Technol.*, vol. 67, no. 11, pp. 10329–10379, Nov. 2018.

[4] Y. Zheng, M. Ouyang, X. Han, L. Lu, and J. Li, "Investigating the error sources of the online state of charge estimation methods for lithium-ion batteries in electric vehicles," *J. Power Sources*, vol. 377, pp. 161–188, Feb. 2018.

[5] X. Zhang, Y. Wang, D. Yang, and Z. Chen, "An on-line estimation of battery pack parameters and state-of-charge using dual filters based on pack model," *Energy*, vol. 115, pp. 219–229, Nov. 2016.

[6] C. Jian, O. Quan, C. Xu, and H. Su, "Neural network-based state of charge observer design for lithium-ion batteries," *IEEE Trans. Control Syst. Technol.*, vol. 26, no. 1, pp. 313–320, Jan. 2018.

[7] T. Hansen and C.-J. Wang, "Support vector based battery state of charge estimator," *J. Power Sources*, vol. 141, no. 2, pp. 351–358, Mar. 2005.

[8] Z. Dong, H. Wang, J. An, C. Jing, H. Pan, and C. Lin, "Real-time estimation of battery state of charge with metabolic grey model and LabVIEW platform," *IEEE Access*, vol. 6, pp. 13170–13180, 2018.

[9] M. Chen *et al.*, "A multilayer electro-thermal model of pouch battery during normal discharge and internal short circuit process," *Appl. Thermal Eng.*, vol. 120, pp. 506–516, Jun. 2017.

[10] X. Hu, S. Li, and H. Peng, "A comparative study of equivalent circuit models for Li-ion batteries," *J. Power Sour.*, vol. 198, pp. 359–367, Jan. 2012.

[11] C. Zou, L. Zhang, X. Hu, Z. Wang, T. Wik, and M. Pecht, "A review of fractional-order techniques applied to lithium-ion batteries, lead-acid batteries, and supercapacitors," *J. Power Sources*, vol. 390, pp. 286–296, Jun. 2018.

[12] L. Zhang, X. Hu, Z. Wang, F. Sun, and D. G. Dorrell, "Fractional-order modeling and state-of-charge estimation for ultracapacitors," *J. Power Sources*, vol. 314, pp. 28–34, May 2016.

[13] X. Hu, F. Sun, and Z. Yuan, "Estimation of state of charge of a lithium-ion battery pack for electric vehicles using an adaptive luenberger observer," *Energies*, vol. 3, no. 9, pp. 1586–1603, 2011.

[14] I.-S. Kim, "The novel state of charge estimation method for lithium battery using sliding mode observer," *J. Power Sources*, vol. 163, no. 1, pp. 584–590, 2006.

[15] Y. Wang, C. Zhang, and Z. Chen, "A method for state-of-charge estimation of $LiFePO_4$ batteries at dynamic currents and temperatures using particle filter," *J. Power Sources*, vol. 279, pp. 306–311, Apr. 2015.

[16] G. L. Plett, "Extended Kalman filtering for battery management systems of LiPB-based HEV battery packs: Part 1. Background," *J. Power Sources*, vol. 134, pp. 252–261, Aug. 2004.

[17] F. Sun, X. Hu, Y. Zou, and S. Li, "Adaptive unscented Kalman filtering for state of charge estimation of a lithium-ion battery for electric vehicles," *Energy*, vol. 36, no. 5, pp. 3531–3540, 2011.

[18] W. Waag, C. Fleischer, and D. U. Sauer, "Critical review of the methods for monitoring of lithium-ion batteries in electric and hybrid vehicles," *J. Power Sources*, vol. 258, pp. 321–339, Jul. 2014.

[19] C. Fleischer, W. Waag, H.-M. Heyn, and D. U. Sauer, "On-line adaptive battery impedance parameter and state estimation considering physical principles in reduced order equivalent circuit battery models: Part 1. Requirements, critical review of methods and modeling," *J. Power Sources*, vol. 260, pp. 276–291, Aug. 2014.

[20] V.-H. Duong, H. A. Bastawrous, K. C. Lim, K. W. See, P. Zhang, and S. X. Dou, "Online state of charge and model parameters estimation of the $LiFePO_4$ battery in electric vehicles using multiple adaptive forgetting factors recursive least-squares," *J. Power Sources*, vol. 296, pp. 215–224, Nov. 2015.

[21] Y. Hu and Y.-Y. Wang, "Two time-scaled battery model identification with application to battery state estimation," *IEEE Trans. Control Syst. Technol.*, vol. 23, no. 3, pp. 1180–1188, May 2015.

[22] Z. Wei, T. M. Lim, M. Skyllas-Kazacos, N. Wai, and K. J. Tseng, "Online state of charge and model parameter co-estimation based on a novel multi-timescale estimator for vanadium redox flow battery," *Appl. Energy*, vol. 172, pp. 169–179, Jun. 2016.

[23] H. Dai, T. Xu, L. Zhu, X. Wei, and Z. Sun, "Adaptive model parameter identification for large capacity Li-ion batteries on separated time scales," *Appl. Energy*, vol. 184, pp. 119–131, Dec. 2016.

[24] Z. Cheng, W. Allafi, Q. Dinh, P. Ascencio, and J. Marco, "Online estimation of battery equivalent circuit model parameters and state of charge using decoupled least squares technique," *Energy*, vol. 142, pp. 678–688, Jan. 2018.

[25] A. Jossen, "Fundamentals of battery dynamics," *J. Power Sources*, vol. 154, pp. 530–538, Mar. 2006.

[26] X. Zhao, Y. Cai, L. Yang, Z. Deng, and J. Qiang, "State of charge estimation based on a new dual-polarization-resistance model for electric vehicles," *Energy*, vol. 135, pp. 40–52, Sep. 2017.

[27] A. Vahidi, A. Stefanopoulou, and H. Peng, "Recursive least squares with forgetting for online estimation of vehicle mass and road grade: Theory and experiments," *Vehicle Syst. Dyn.*, vol. 43, no. 1, pp. 31–55, 2005.

[28] T. R. Fortescue, L. S. Kershenbaum, and B. E. Ydstie, "Implementation of self-tuning regulators with variable forgetting factors," *Automatica*, vol. 17, pp. 831–835, Nov. 1981.

[29] A. E. Bryson, Y.-C. Ho, and G. M. Siouris, "Applied optimal control: Optimization, estimation, and control," *IEEE Trans. Syst., Man, Cybern.*, vol. 9, no. 6, pp. 366–367, Jun. 2007.

[30] L. Lu, X. Han, J. Li, J. Hua, and M. Ouyang, "A review on the key issues for lithium-ion battery management in electric vehicles," *J. Power Sour.*, vol. 226, pp. 272–288, Mar. 2013.

[31] *USABC Electric Vehicle Battery Test Procedures Manual. Revision 2*, Office of Scientific & Technical Information, 1996.

[32] F. Baronti *et al.*, "Parameter identification of Li-Po batteries in electric vehicles: A comparative study," in *Proc. IEEE Int. Symp. Ind. Electron.*, May 2013, pp. 1–7.

[33] Y. Gao and M. Ehsani, "Design and control methodology of plug-in hybrid electric vehicles," *IEEE Trans. Ind. Electron.*, vol. 57, no. 2, pp. 633–640, Feb. 2010.

SHIQI LIU received the B.Sc. degree from Wuhan University, in 2017, where he is currently pursuing the Ph.D. degree. His main research interests include lithium battery characteristics, battery management system in electric vehicles, and battery balance management systems.

JUNHUA WANG was born in Linyi, Shandong, China, in 1981. He received the Ph.D. degree from The Hong Kong Polytechnic University, Hong Kong, in 2012. In 2012, he joined the GATE Center for Electric Drive Transportation, Carnegie Mellon University, MI, USA, as a Postdoctoral Researcher and then a Research Fellow. He is currently a Professor with the School of Electrical Engineering, Wuhan University. His main research interests include wireless transmission technology based on magnetic resonance, applied electromagnetics, and system equipment for power transmission and distribution.

QISHENG LIU was born in Wuhan, Hubei, China, in 1962. He received the B.S. degree in electric-machinery from Hunan University, Changsha, China, in 1984, and the M.S. degree in high-voltage and the Ph.D. degree in power system and automation from Wuhan University, Wuhan, in 1992 and 2006, respectively, where he is currently an Associate Professor with the School of Electrical Engineering. His research interests include power system operation and control, battery charger, and renewable energy applications.

JIA TANG received the bachelor's degree from Wuhan University, in 2017. His research interests include lithium battery characteristics, battery state estimation, and fault detection in electric vehicles.

HAOLU LIU is currently pursuing the bachelor's degree with Wuhan University. Her main research interests include lithium battery characteristics and battery management systems in electric vehicles.

ZHIJIAN FANG was born in Nanzhang, Hubei, China, in 1988. He received the B.S. and Ph.D. degrees in electrical engineering from the Huazhong University of Science and Technology, Wuhan, China, in 2010 and 2015, respectively. From 2015 to 2018, he was a Lecturer with the School of Electrical Engineering and Automation, Wuhan University. From 2016 to 2017, he was a Postdoctoral Research Fellow of the Department of Electrical and Computer Engineering, Ryerson University, Toronto, Canada. Since 2018, he has been a Professor with the School of Automation, China University of Geosciences, Wuhan. His research interests include high-performance DC/DC converter, battery charger, renewable energy applications, and wireless power transmitter.